4.1. Introduction

Heterocyclic conducting polymers with mesoscale crystallization ability have extensively studied in electronic devices due to high charge mobility in their self-ordered form [Yang et al. (2016), Karatrantos et al. (2016), Wie et al. (2014), Yang et al. (2005)]. Regioregular poly (3-hexylthiophene) (rr-P3HT) has considered as prominent material to fulfill these criteria. Apart from rr-P3HT, regioregular poly (3,3’’’-didodecylquarter thiophene) (rr-PQT-12) has been also widely used as alone or in composite form as active material in various applications like FET, diodes, sensors or insolar cells, owing to the combination of their electrical, mechanical and optoelectronic properties [Tremel et al. (2014), Newbaloom et al. (2011), Lee et al. (2010), Bilgaiyan et al. (2015), Chang et al. (2016), Meng et al. (2014), Pandey et al. (2014)]. It is now well known that one of the crucial factors for charge carrier mobility in organic polymers is crystallinity and chains orientation in a successive fashion (collectively called ordered orientations) [Kline et al. (2006), Dou et al. (2014), Li et al. (2016)] so that carriers can hop through well connected crystalline regions. This type of orientations occurs only if coiled unimers adopt an extended conformation by possible orientation in preferable conditions. For example, due to rigid thiophene backbone favours π-π intermolecular interaction predominantly in one dimension like rr-P3HT that favours better electrical properties. That is why the self-assembly of this polymer may give a breakthrough methodology for the enhancement in the properties of materials. Apart from this, self-assembled semiconducting polymers have segmental electronic traps within the stacks of polymer chain, results the favorable charge transport by hopping or band transport [Wu et al. (1991)]. Enormous efforts like aging, ultra-sonication, thermal annealing, pressure dependent assembly solution, aggregation on lyophilic solvent surfaces (floating film

transfer method) and vaporization technique have been applied for the ordering of the semiconducting polymers mainly P3HT [Sun et al. (2015), Byun et al. (2009), Pandey et al. (2014), Pandey et al. (2013), Pandey et al. (2015), Bhargava et al. (2016), Pandey et al. (2013), Rubi et al. (2015), Acevedo-Cartagena et al. (2015)]. Apart from this some other controlled technique has also been applied for the ordering of several polymers which is liable to better charge transfer properties [Li et al. (2016), Joshi et al. (2012), Gupta et al. (2012), Gupta et al. (2010)]. However, there is no report available on time dependent aggregation of rr-PQT-12 in marginal solvent at room temperature and its usage as an active material in diode fabrication at optimal conditions. In this paper, we report solvent driven optimization of fibril growth of rr-PQT-12 in chloroform and its charge transfer properties by fabricating Schottky diode compared to that of its isolated analogue (un-aggregated rr-PQT-12).

4.2. Experimental

4.2.1. Materials

Polymer, rr-PQT-12 (Lot#14K007B1) molecular weight = 15,000–50,000 & HOMO = 5.24 eV & LUMO = 2.97 eV) was purchased from American Dye Source, Inc. USA and chloroform (analytical grade) was purchased from Merck, India.

4.2.2. Optimization of rr-PQT-C12 fibril formation

For the optimization of fiber formation, 0.125%, 0.055% and 0.026% w/v rr-PQT-12 solutions were chosen for the study. In this process, a stock solution of 0.5% w/v rr-PQT-12 was prepared with chloroform in sealed glass vials and completely dissolved by heating at 80^{o}C. After complete dissolution, 250µL of this stock solution was further diluted by 750µL

chloroform for the preparation of 0.125%w/v rr-PQT-12 and allowed to spontaneous cooling for 10 minute to get 25^{o}-27^{o}C in a temperature controller equipped closed chamber. This particular solution is referred as 'isolated rr-PQT-12' during whole experimentation. After that this solution was kept 45 minute to insure fiber formation which is justified by UV-visible spectrum (**Fig. 4.2** (II)). As soon as time passes the colour of rr-PQT-12 solution changes from light orange to reddish-brown due to self-assembly of polymer chains (as shown in inset of **Fig. 4.2** (I)). Similar procedures were applied with the help of UV-visible analysis for rest concentrations of rr-PQT-12 solution to compare the self-assembly of polymer chains.

4.3. Results and discussion

It is previously reported that due to numerous conformational degree of freedom and segmental partially filled sp^2 hybrid orbitals (loosely bound π-orbitals), conducting polymers tend to self-assemble into a favorable microstructure that mainly depends upon applied conditions [Groschel et al. (2012)]. Particularly, in solution state, due to low saturating concentration, these polymers are capable of self-assembly when subjected to gradual decrement in temperature. Herein, individual unimers act as template for the other molecules [Samitsu et al. (2008)].Similar to rr-P3HT, there are two types of self-assemblies can also be possible for rr-PQT-12 viz. one along a-axis and other along b-axis which is abbreviated as H and J aggregates respectively (as schematically represented in **Fig. 4.1**)[22-24]. On the other hand, chain folding plays crucial role for the conformation of individual unimers. For example, rr-PQT-12 exhibits loosely packed aggregated chain conformations into fiber than rr-P3HT due to rigidness of quarter thiophene backbone [Hu et al. (2013)]. That is why rr-P3HT shows aggregation by folding of chains while rr-PQT-12 exhibits non folding

aggregation into fiber. Herein, we are studying charge transport properties of non-folded rr-PQT-12 fiber compared to its isolated analogue by various tools as describe one by one. The evidence of self-assembly is monitored by UV visible, PL, AFM and TEM.

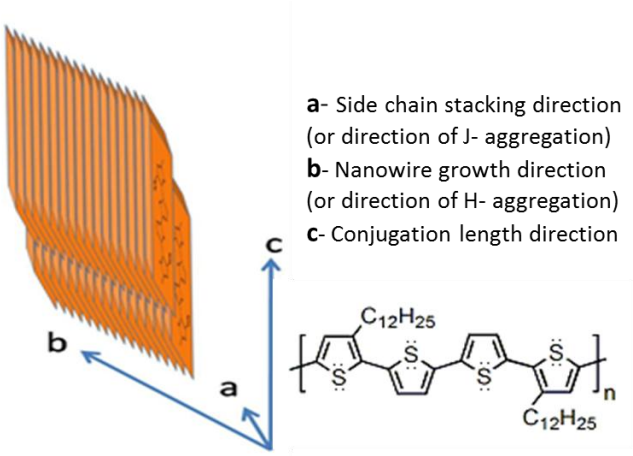

Fig. 4.1. Schematic representation for H-and J-aggregation in rr-PQT-12 (PQT-12 chain is shown at bottom).

UV-visible analysis:

The aggregation of rr-PQT in chloroform is observed by UV-visible as shown in **Fig. 4.2**. In order to better presentation, UV-visible curves were normalized with respect to maximum absorbance i.e.at 473 nm in **Fig. 4.2** (I). The maximum absorption peak at 473nm in the Isolated rr-PQT-12 exhibits due to π-π* transition in either concentration. However, upon ageing, one shoulder peak at 603nm is appeared due to coupling of π-π* transition to the C=C stretching in the thiophene ring like P3HT (*cf.* **Fig. 4.2** Ia, Ib and Ic with that of Ia', Ib'and Ic') [Sundberg et al. (1989), Spano (2005)]. This shoulder peak goes on increasing with increase in concentration as well as with passage of time due to self-assembly of polymer causes change in optical density.

After that the peak intensity observed at 603nm is again compared for all concentrations to passage of time and their analysis is shown in **Fig. 4.2** (II). The correlation of fiber formation is observed using time dependent absorption analysis (kinetic study at peak intensity=603 nm), monitored automatically up to 850 minutes with the interval of 2 minute. In all cases, the shoulder peak gradually increases till a particular period of time and then decreases and then starts to increase like initial case due to settling of as-assembled polymer and starting of new aggregation phenomenon. Herein exact time is determined by intersection of tangents corresponding to maximum absorption. For example, in case of 0.125% w/v rr-PQT-12, upto 45 min absorption increases and then decreases to 715 min. After that the shoulder peak again starts to increase due to further growth of new chain assembly. Similarly0.055% w/v rr-PQT-12 shows gradual increment in absorption intensity till 80 and then decreases to 183 minute and further increases. 0.026% w/v rr-PQT-12 exhibit decrease in absorption intensity at 580 minute and then decreases like others. Apart from these evidences, the nature of curve is different for either case of studies due to difference in the rate of settling ability of as-aggregated fibers and growth of new fibers simultaneously that is responsible for alteration in whole optical density of dispersion. Herein, we have chosen 45, 80 and 580 minutes for optimal ageing time of 0.125%, 0.055% and 0.026% w/v of rr-PQT-12 dispersion respectively for the further case of study.

The evidence of fiber formation was further justified by photoluminescence emission analysis excited at 473 nm for similar concentrations of rr-PQT-12 solution in chloroform. Change in the emission intensity (quenching) is attributed to the dense packing and molecular orientation, effectively along fiber axis (b-axis).The measure of exciton diffusion length was compared with the help of Spano's model equation (1) [Spano (2005)].

$$\frac{I_{0-0}}{I_{0-1}} \approx \frac{1}{2e^{-2}} \left(\frac{1-0.24^{W}/_{E_p}}{1-0.39^{W}/_{E_p}} \right)^2 \frac{\sigma^2}{W^2} \quad (1)$$

Here 'W' is exciton bandwidth, 'E_p' is energy of main intramolecular vibration couples to electronic transition and 'σ' is the measure of disorder and it is directly proportional to the ratio of I_{0-0} and I_{0-1}.

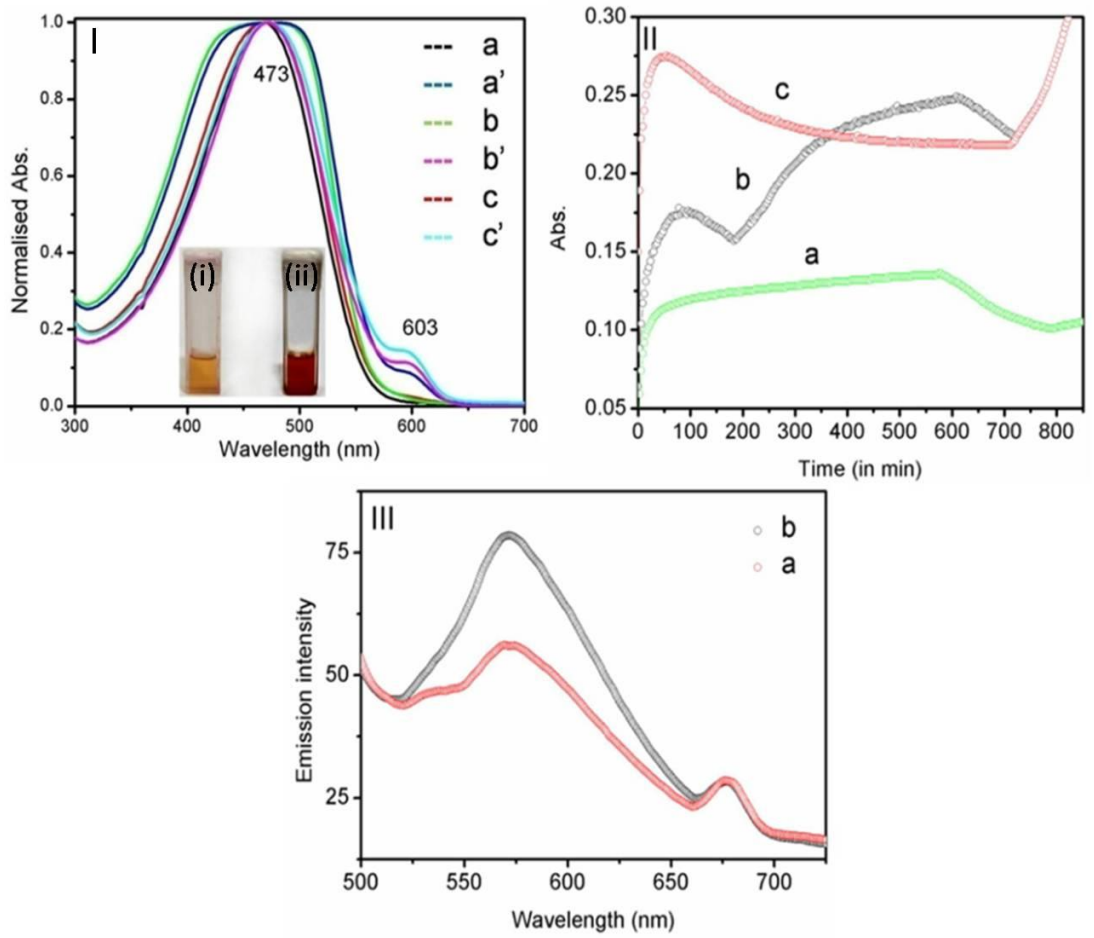

Fig. 4.2. (I) UV-visible analysis of isolated (a, b and c) and aggregated (a', b' and c') rr-PQT-12 for 0.026%, 0.055% and 0.125% w/v respectively, (II) Time dependent absorbance analysis of (a) 0.026% w/v, (b) 0.055% w/v and (c) 0.125% w/v in chloroform and (III) PL of (a) aggregated and (b) isolated rr-PQT-12 excited at 473 nm. Inset of **Fig. 4.2**(I) represents photograph of change in colour of rr-PQT-12 solutions from zero time (isolated) marked as (i) and after 45 minutes aging (aggregated) marked as (ii).

This ratio is estimated from **Fig. 4.2** (III) as 2.76 and 1.97 for isolated and aggregated rr-PQT-12, respectively, indicating the decrease in level of disorder whenever aggregations take place. This evidence was further verified by XRD as discussed latter.

XRD analysis:

The directionality of chain assembly was ascertained by XRD as shown in **Fig. 4.3** and their peaks are isolated by deconvolution process. Isolated rr-PQT-12 exhibit loosely packed structure with two distinct peaks at 2θ=4.45° and 22° corresponding to side chain interaction along (100) plane and π-π orientation along (010) plane [Ong et al. (2004), Ong et al. (2005)]. While two diffraction peaks at 2θ= 11.2° along (200) plane and 16.5° along (300) plane are corresponding to second and third order reflection peaks respectively. However, on aggregation the intensity of (100) plane increases due to growth of fiber along b-axis while other peaks remain same.

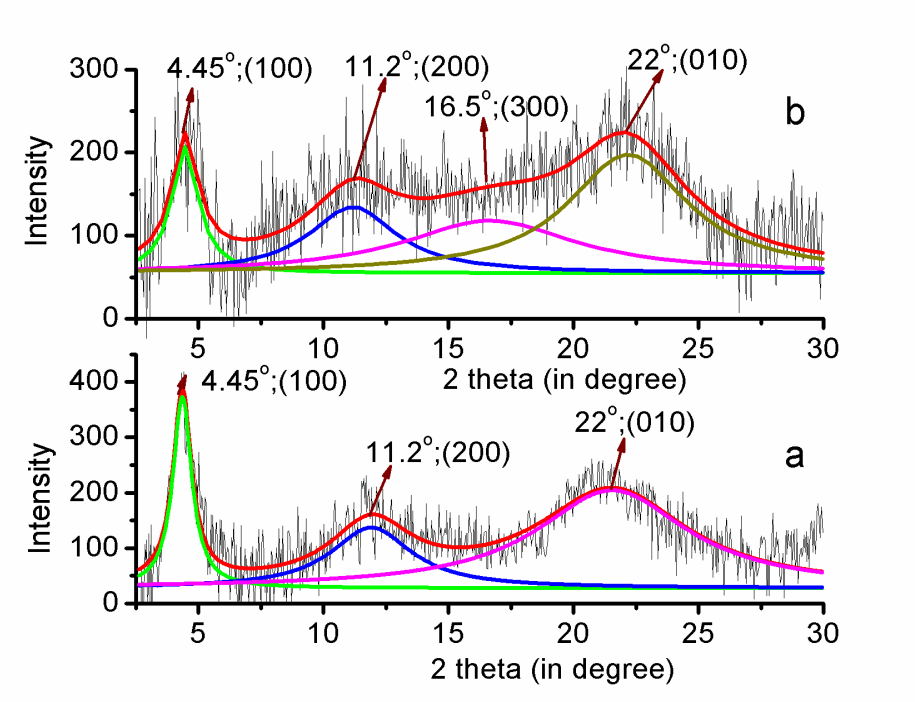

Fig. 4.3. XRD of (a) aggregated and (b) isolated rr-PQT-12.

4.3.3. Morphological properties: AFM analysis

The fibril morphology in case of rr-PQT-12, is also a signature of individual ordering chain by π-π stacking along the perpendicular to the backbone axis similar to that of region regular P3HT [Kumar et al. (2014)]. AFM image of different rr-PQT-12 film along with its corresponding height profile is shown in **Fig. 4.4**.

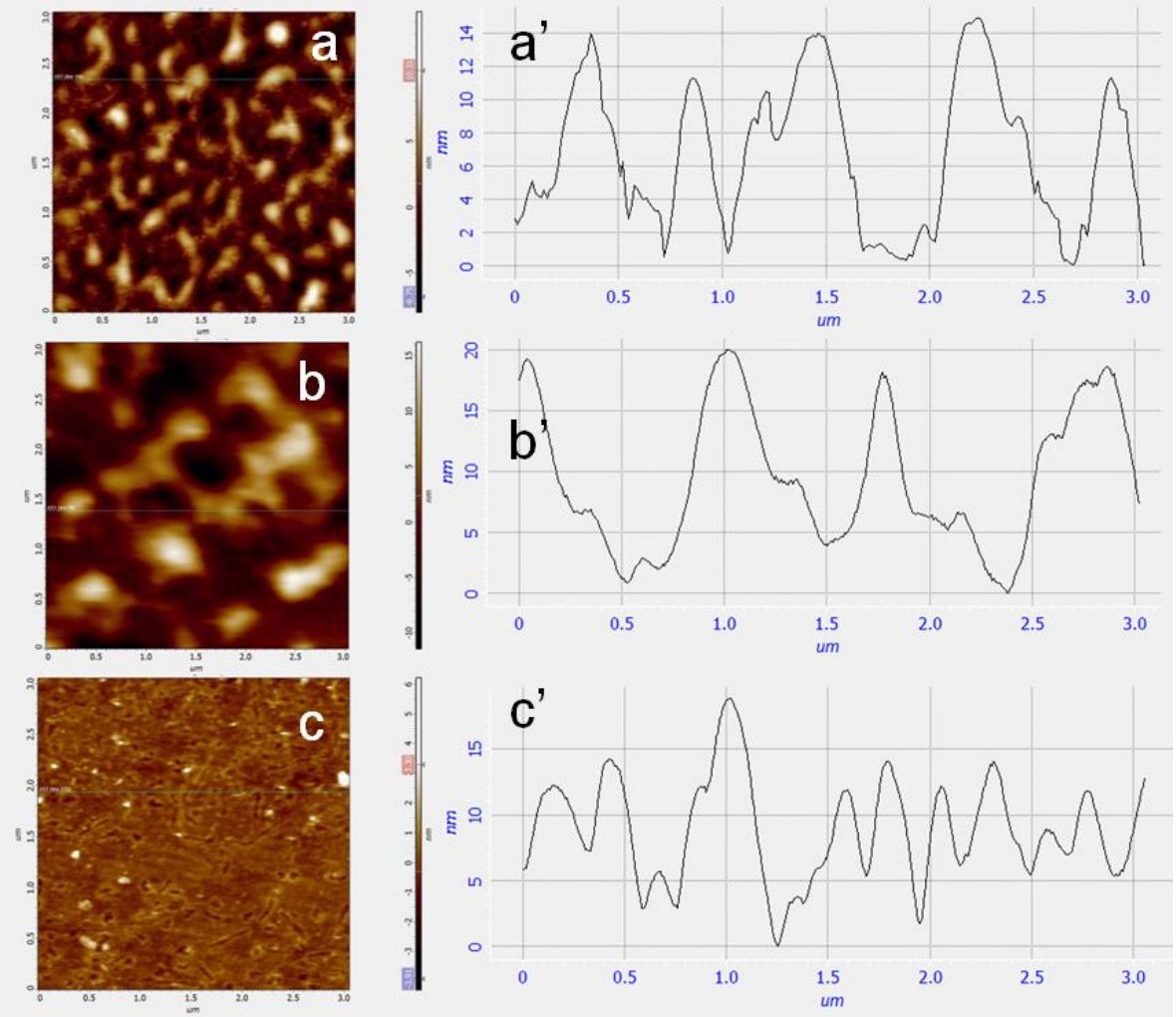

Fig. 4.4. AFM image and their corresponding height of 0.026% w/v rr-PQT-12 (a & a'), 0.055% w/v rr-PQT-12 (b & b') and 0.125% w/v rr-PQT-12 (c & c').

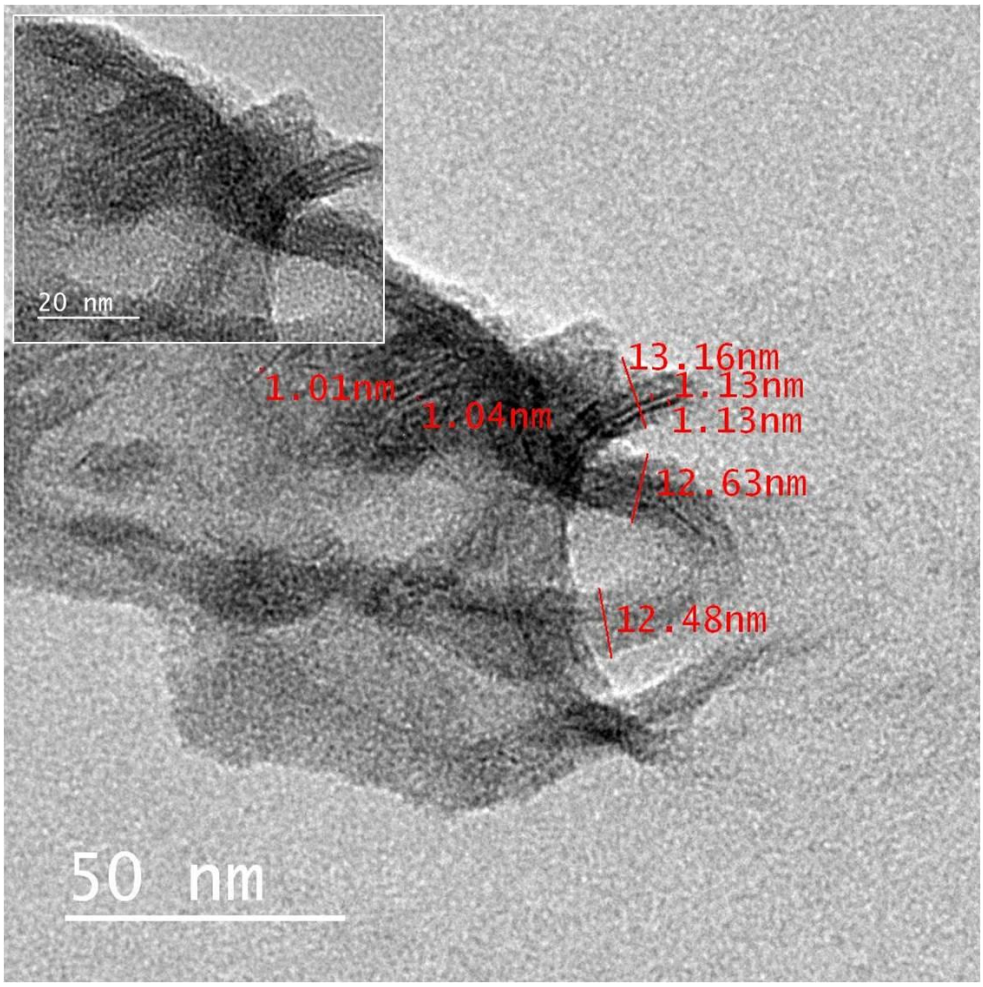

Fig. 4.5. HRTEM image of fibrous rr-PQT-12. Inset shows zoomed view of same micrograph.

Approximately same film thickness of rr-PQT film is coated on glass plate by spin cast method (rpm=2000, 40s) from different aged dispersion (at 45, 80 and 580 minutes). Herein we observed well resolved fibril assembly in nanometric range (from 35-50 nm) for the case of 0.125% w/v rr-PQT12, while irregular embryos for assembly of other rr-PQTs are formed. It means these lower concentrations are not sufficient for the fiber growth. On further resolution of individual fibers, we observed that these nanometric fibers are already a bundle of small fibers of ~12 nm (as shown in **Fig. 4.5**).

Fabrication of device and study of charge transport properties:

The device function behavior related to charge transport properties of rr-PQT-12 fiber and its isolated form were studied by making a contact as shown in inset of **Fig. 4.6**. Both aggregated and isolated rr-PQT-12 exhibits unsymmetrical current response under the applied potentials across this contact. Various parameters were correlated with isolated rr-PQT-12 film. All device parameters were calculated using ideal diode equation based on thermionic emission theory as explained elsewhere [Heeger et al. (1994)] and summarized in **Table 4.1**. On comparing the response of similar range of applied voltage on as-fabricated devices, the device fabricated using rr-PQT-12 fiber exhibits high current density (about ten times higher) with high rectification ratio (five times higher) even on almost similar barrier heights compared to that of isolated rr-PQT-12. This is due to the entrapment of charges within aggregated region [Duong et al. (2012)]. However, the deviation of η from its ideality is due to trap assisted tunneling, carrier leakage and inhomogeneous barrier [Rose (1955)].

In order to explain conduction mechanism and charge mobility, the curves of **Fig. 4.6**(I) are replotted in a double logarithmic J-V form as shown in **Fig. 4.6**(II). These curves exemplify three well explain regions (for isolated marked as A, B and C and for aggregated marked as A', B' and C') corresponding to Ohmic, trap filled space charge limited current and trap free space charge limited current regions respectively [Nikitenko et al. (2003)]. Particularly, region B or B' is described by power law, in which it is assumed that filling of trap distribution occur exponentially and is maximum density near the band edge. Since the slop of B' is higher than B, therefore trap filling distribution is abrupt in case of B', while it is gradual in B-region (1.8 *vs* 0.6). Further it is believed that, approximately all trapping centers are occupied by injected charge carriers on/after the intersection of B- and C-regions

[Nikitenko et al. (2003), Chiguvare et al. (2004)] and current density increases exponentially with short applied voltage range. Thus charge carrier mobility, μ of charge carriers is calculated by Mott-Gurney's equation by assuming completely filled traps [Pasveer et al. (2005)].

$$J = \frac{9}{8}\varepsilon\mu\frac{V^2}{d^3} \quad (2)$$

Where J is current density (in mA/cm^2), V is voltage (in V) applied across the film, d is thickness (in nm) of film and ε is dielectric permittivity of film and it is taken as1.94 [Porrazzo et al. (2015)]. We observed the forwards current and mobility in rr-PQT-12 fiber is 10 times higher than that of its isolated analogue. This is due to the direct consequence of aggregation of chain along face-on-direction that favors inter chain free charge conduction by hopping process [Tiwari et al. (2014)].

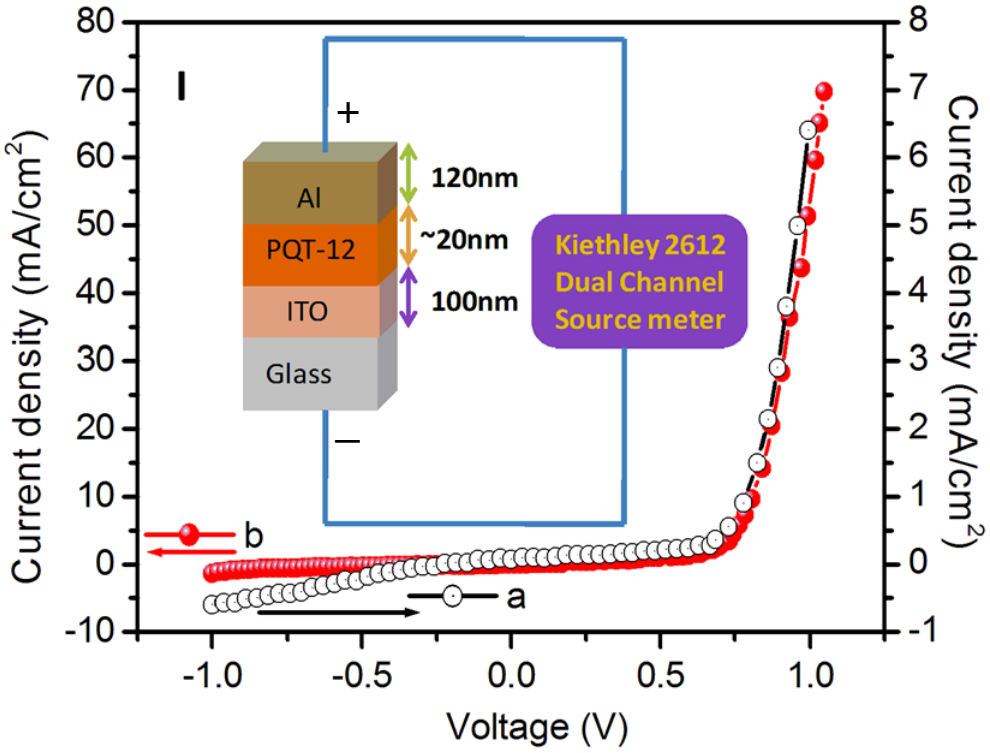

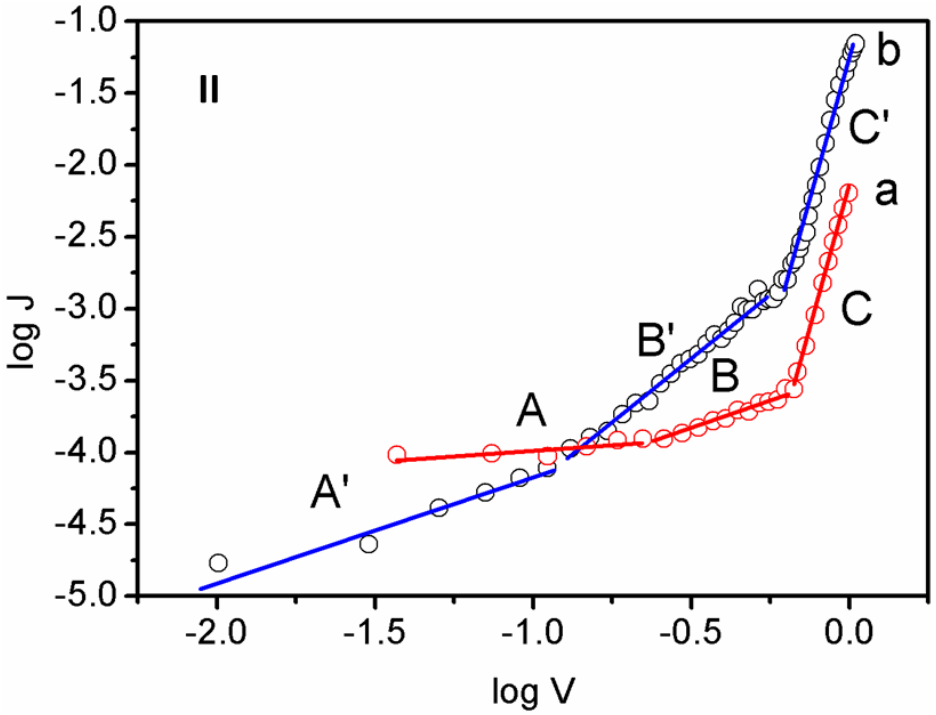

Fig. 4.6. (I) J-V Characteristics and (II) log-log J-V plot of (a) isolated and (b) aggregated rr-PQT-12. Inset shows the device schematic diagram.

Table 4.1. Device parameters of as-fabricated devices.

Parameters	**Al/Aggregated rr-PQT-12 /ITO**	**Al/Isolated rr-PQT-12/ITO**
Forward current density @1V(in mA/cm^2)	69.0	6.4
Leakage current density J_o(in mA/cm^2)	2.12×10^{-4}	3.57×10^{-4}
Ideality factor (η)	3.05	3.89
Barrier height (φ_B) (in eV)	0.69	0.68
Reverse current density @-1V(in mA/cm^2)	-1.38	-0.06
Rectification Ratio	50.00	10.77
Mobility (in cm^2/Vs)	1.58 x 10^{-10}	2.13 x 10^{-11}

4.4. Conclusions

The experimental observations presented here exemplify that rr-PQT-12 concentration plays important role for their assembly into fiber form and 45 minute is sufficient for the assembly in case of 0.01% w/v rr-PQT-12 in chloroform. The fiber growth direction predominantly occurs toward theπ-π stacking (b-axis). This strategy enables 10-m increment in forward current density with high rectification ratio even on similar barrier heights compared to that of the isolated rr-PQT-12 (69.0 mA/cm^2*vs.*6.4mA/cm^2).This is due to the formation of π-stacked aggregate favours charge trapping.

This study provides a fruitful insight into the role of ordering of rr-PQT-12 isolated chain in chloroform solvent and its impact to organic electric devices. The optimization analysis will create future opportunities for high performance electron transport devices.